FULL PAPERS

Controlled Self-Assembly of Functional Metal Octaethylporphyrin 1D Nanowires by Solution-Phase Precipitative Method

Man-Ho So, V. A. L. Roy, Zong-Xiang Xu, Stephen Sin-Yin Chui, Mai-Yan Yuen, Chi-Ming Ho, and Chi-Ming Che*[a]

Abstract: Metal octaethylporphyrin M-(OEP) (M = Ni, Cu, Zn, Pd, Ag, and Pt) nanowires are fabricated by a simple solution-phase precipitative method. By controlling the composition of solvent mixtures, the diameters and lengths of the nanowires can be varied from 20 to 70 nm and 0.4 to 10 μm, respectively. The Ag(OEP) nanowires have lengths up to 10 μm and diameters of 20–70 nm. For the M-(OEP) nanowires, the growth orientation and packing of M(OEP) molecules are examined by powder XRD and SAED measurements, revealing that these M(OEP) nanowires are formed by the self-assembly of M(OEP) molecules through intermolecular π···π interactions along the π···π stacking axis, and the M^{2+} ion plays a key role in the nanowire formation. Using the bottom contact field effect transistor structure and a simple drop-cast method, a single-crystal M(OEP) nanowires-based field effect transistor can be readily prepared with prominent hole transporting behaviour and charge-carrier mobility up to 10^{-3}–10^{-2} $cm^2 V^{-1} s^{-1}$ for holes, which are 10 times higher than that of vacuum-deposited M-(OEP) organic thin-film transistors (OTFTs).

Keywords: nanostructures · nanowires · porphyrinoids · self-assembly · stacking interactions

Introduction

Nanomaterials such as nanoparticles, nanowires and nanotubes have demonstrated useful applications in catalysis, electronics, and biological studies.[1] Of particular interest to us is one dimensional (1D) nanowires and nanotubes, which have strong anisotropic growth properties, excellent single crystallinity, and unique electronic and optical properties.[2] Recently, self-assembled organic nanomaterials have inspired a surge in research interest, arising from their flexibility, nonlinear optical effects, high photoconductivity and promising applications in electronic and optical nanodevices.[2d–g] 1D organic nanowires, such as those of metal phthalocyanines,[3] perylene derivatives,[4] and oligoacene derivatives,[5] are usually prepared by self-assembly processes, with the molecules being held together by intermolecular π···π interactions and growing anisotropically along the π···π stacking axis. More recently, we have shown that self-assembled 1D organometallic nanowires can be obtained and grown anisotropically resulting from intermolecular Pt···Pt interactions.[6] These chain-like intermolecular Pt···Pt interactions guide the assembly and stacking of the Pt^{II} organometallic complexes in a linear manner, resulting in anisotropic growth of the nanowires along the axis of Pt···Pt interactions.

Metalloporphyrins are an important class of metal complexes that have been studied in many fields including catalysis, biochemistry, electrochemistry, and photochemistry.[7] They are well-documented to display intermolecular π···π interactions in the solid state and have recently been extensively studied in the context of the preparation of nanostructures. Examples of nanostructures prepared from free porphyrin or metalloporphyrin include nanoparticles,[8] nanowires,[9] nanotubes,[10] nanorings,[9c,11] and nanosheets.[12] The water-soluble porphyrins, *meso*-tetrakis(4-sulfonatophenyl)-porphyrin diacid form ($[H_4TPPS_4]^{2-}$),[9a–b,13] and *meso*-tetrakis(4-carboxyphenyl)porphyrin diacid form ($[H_4TCPP]^{2+}$),[9c] individually can assemble into 1D nanostructures by acid-induced aggregation. The self-assembly reaction between anionic $[H_4TPPS_4]^{2-}$ and cationic Sn^{IV} *meso*-tetrakis(4-pyri-

[a] M.-H. So, Dr. V. A. L. Roy, Z.-X. Xu, Dr. S. S.-Y. Chui, M.-Y. Yuen, Dr. C.-M. Ho, Prof. C.-M. Che
Department of Chemistry and the HKU-CAS Joint Laboratory on New Materials,
The University of Hong Kong,
Pokfulam Road, Hong Kong SAR (China)
Fax: (+852) 2857-1586
E-mail: cmche@hku.hk
Supporting information for this article is available on the WWW under http://dx.doi.org/10.1002/asia.200800162.

dyl)porphyrins ([Sn(OH)$_2$TPyP]$^{4+}$ and [Sn(OH)-(H$_2$O)TPyP]$^{5+}$) leads to the formation of nanotubes.[10a,b] Additionally, Zn^{II} *meso*-tetrakis(4-pyridyl)porphyrin (ZnTPyP) can self-assemble into 1D tube-like hollow hexagonal nanoprisms in the presence of the surfactant cetyltrimethylammonium bromide.[10c] In addition, the vapor diffusion method has also been reported to induce self-assembly of molybdenum(V) dodecaphenylporphyrin [Mo(DPP)(O)-(H$_2$O)]$^{+}$ into nanotubes.[10d] All these literature reported metalloporphyrins and porphyrins used for nanostructure formation have phenyl or pyridyl substitutents at the *meso*-position of the porphyrinato ring,[14] which hinder direct intermolecular interactions between porphyrin molecules.

Planar metal octaethylporphyrins (M(OEP)) are sterically unencumbered. Intermolecular π···π interactions between M(OEP) (for M = Ni, Cu, and Zn) molecules in the solid state have been reported.[15] Devices such as organic thin-film transistors (OTFTs),[16] organic light-emitting devices (OLEDs),[17] and organic solar cells[18] based on thin films of metal octaethylporphyrins, have already been documented. Yet, the preparation and applications of M(OEP) nanowires have not been narrated in the literature. Herein, we demonstrate the self-assembly of M(OEP) (where M = Ni, Cu, Zn, Pd, Ag, and Pt) molecules into functional 1D nanowires. The M(OEP) nanowires studied in this work can be fabricated at ambient conditions by a simple precipitative method.[4f,19] No surfactant or template is needed to assist the fabrication of nanowires. The size of the nanowires can be controlled by changing the composition of solvent mixtures. We have examined the growth, orientation, and crystal packing of M(OEP) molecules that lead to the formation of 1D nanowires. The divalent metal cation in the octaethylporphyrin ring results in a larger extent of "face-to-face" stacking and better overlap of M(OEP) molecules by intermolecular π···π interactions in comparison with free octaethylporphyrin (H$_2$OEP) molecules. Compared to the bulk thin film counterparts, these M(OEP) nanowires exhibit substantially better charge transporting properties.

Results and Discussion

The chemical structure of octaethylporphyrin and metalloporphyrins studied in this work are depicted in Figure 1. Ni-(OEP), Cu(OEP), Pd(OEP), and the free base H$_2$OEP were purchased from commercial sources. Ag(Por) (Por = *meso*-tetraphenylporphyrin (TPP), *meso*-tetrakis(4-tolyl)porphyrin (TTP) and OEP dianions),[20] Zn(OEP),[15c] Pt(OEP),[21] and [Au^{III}(OEP)]Cl,[22] were synthesized according to the literature methods with some modifications. Ag(F$_{20}$TPP) was synthesized by reacting *meso*-tetrakis(pentafluorophenyl)porphyrin (H$_2$F$_{20}$TPP) with AgNO$_3$ in acetic acid under reflux conditions. The ORTEP drawing and crystal data of Ag-(F$_{20}$TPP) are shown in Figure 2 and Table 1, respectively.

In the initial experiments, M(OEP) nanowires were prepared by injecting a THF solution containing M(OEP) (100 μM, 1 mL) to H$_2$O (9 mL). The molecular packing in
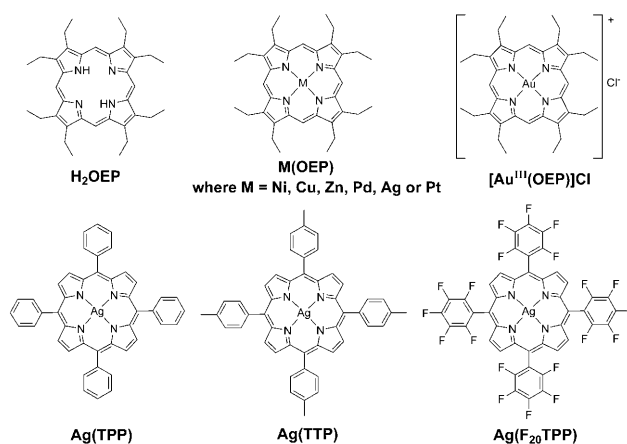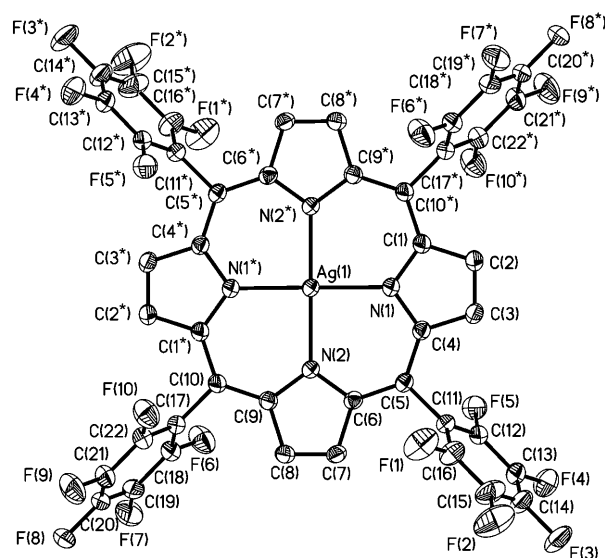

Figure 1. Chemical structures of octaethylporphyrin and metalloporphyrins.

Figure 2. ORTEP drawing of Ag(F$_{20}$TPP) with atom-numbering scheme. Hydrogen atoms are omitted for clarity. The ORTEP drawing of the molecule is made with thermal ellipsoids at the 30% probability level. Selected bond distances (Å): Ag(1)-N(1/1*), 2.082(2) and Ag(1)-N(2/2*), 2.085(2). Selected bond angles (°): N(1*)-Ag(1)-N(1), 180.00(15); N(1*)-Ag(1)-N(2), 89.48(9); N(1)-Ag(1)-N(2), 90.52(9); N(1*)-Ag(1)-N(2*), 90.52(9); N(1)-Ag(1)-N(2*), 89.48(9), and N(2)-Ag(1)-N(2*), 180.0(2).

the M(OEP) nanowires were examined by powder XRD and the results are depicted in Figure 3 (see also Supporting Information, Figure S1). Remarkably, the XRD pattern of M(OEP) (M = Ni, Cu, Zn, Pd, Ag, and Pt) nanowires individually shows two intense diffraction peaks at around 2θ values of 7.22° and 7.96°. To study the XRD pattern of M-(OEP) nanowires in more detail, we retrieved the X-ray crystal structure data of Ni(OEP), Cu(OEP), and Zn(OEP) from the literature,[21] and simulated their XRD patterns. These three M(OEP) (M = Ni, Cu, and Zn) samples are isostructural to each other and Ni(OEP) was used as a reference. Our simulation showed that the peak with a 2θ value of 7.22° (d = 12.26 Å) resembled the calculated positions of

FULL PAPERS

Table 1. Crystal data and structure refinement for $Ag(F_{20}TPP)$

|	$Ag(F_{20}TPP)$
empirical formula	$C_{44}H_8AgF_{20}N_4$
molar mass [g mol^{-1}]	1080.41
temperature [K]	301(2)
wavelength [Å]	0.71073
crystal system	trigonal
space group	$R\bar{3}$
unit cell dimensions	
a [Å]	20.379(4)
b [Å]	20.379(4)
c [Å]	24.627(5)°
α [°]	90
β [°]	90
γ [°]	120
V [Å^3]	8858(3)
Z	9
ρ_{calc} [Mg m^{-3}]	1.823
absorption coefficient [mm^{-1}]	0.648
$F(000)$	4743
crystal size [mm^3]	$0.4 \times 0.3 \times 0.15$
range of θ [°]	2.00–25.67
index ranges	$-24 \leq h \leq 19, -15 \leq k \leq 24,$ $-30 \leq l \leq 29$
reflections collected	16763
independent reflections	3743 [$R_{int} = 0.0176$]
completeness [%] to θ	100.0
absorption correction	none
refinement method	full-matrix least-squares on F^2
data/restraints/parameters	3743/0/313
GOF on F^2	1.072
final R indices [$I > 2\sigma(I)$]	$R1 = 0.0308, wR2 = 0.0730$
R indices (all data)	$R1 = 0.0471, wR2 = 0.0857$
largest diff. peak and hole [e Å^{-3}]	1.702, −0.301
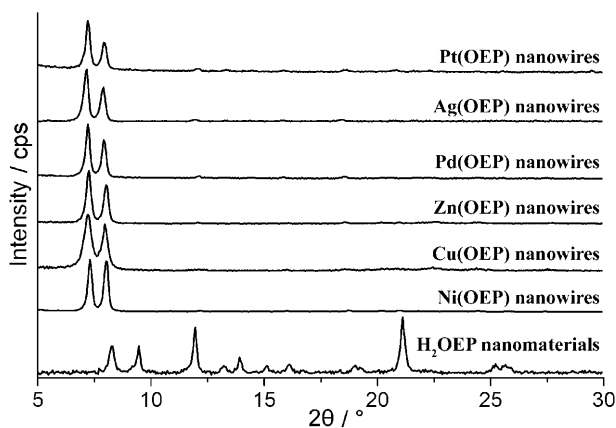
Figure 3. Powder XRD patterns of M(OEP) nanowires.

the [010] ($2\theta = 7.232°$) and [100] ($2\theta = 7.262°$) Miller planes of the crystal structure of Ni(OEP), whereas another peak with a 2θ value of 7.96° ($d = 11.12$ Å) corresponded to the calculated position of the [1-10] ($2\theta = 7.933°$) Miller plane of the crystal structure of Ni(OEP). These two characteristic peaks indicated that these M(OEP) nanowires have a strong preferred molecular orientation in which the [100], [010], and [1-10] Miller planes of the crystal structure of Ni(OEP),

Cu(OEP), and Zn(OEP) are parallel to the plane of the silicon wafer substrate. The XRD patterns of Pd(OEP), Ag-(OEP), and Pt(OEP) nanowires individually revealed the presence of intense peaks at 2θ values of 7.22° and 7.96°, similar to the XRD patterns obtained from Ni(OEP), Cu-(OEP), and Zn(OEP) nanowires (Figure 3). These results revealed that the packing of M(OEP) molecules in these nanowires exhibits a high degree of structural resemblance to that found in the X-ray crystal structures of M(OEP). Also, these results demonstrate that the packing of Pd-(OEP), Ag(OEP), and Pt(OEP) molecules in the nanowires adopt a similar arrangement to that found in the reported crystal structures of Ni(OEP), Cu(OEP), and Zn(OEP).[15] The appearance of intense peaks from the [100], [010], and [1-10] Miller planes indicate that all the M(OEP) (M = Ni, Cu, Zn, Pd, Ag, and Pt) nanowires formed at a fast aniso-tropic growth rate along the [001] direction, which is the c-axis of the crystal structure of Ni(OEP). The growth direction of the nanowires is subsequently confirmed by selected area electron diffraction (SAED) analysis on a single nano-wire (see discussion below). The XRD pattern of H$_2$OEP prepared under the same conditions did not show the two diffraction peaks at 2θ values of 7.22° and 7.96° (Figure 3). Instead, a polycrystalline solid sample of H$_2$(OEP) was formed as evidenced by close matching between the experi-mental and simulated XRD patterns (see Supporting Infor-mation, Figure S1 g). Interestingly, the as-synthesized solid sample of Pt(OEP) contained a mixture of two crystalline phases, as revealed by four diffraction peaks (2θ values of 7.24°, 7.95°, 8.84°, and 9.60°; see Supporting Information, Figure S1 f). The first two peaks matched the peaks position of the [100]/[010] ($2\theta = 7.24°$) and [1-10] ($2\theta = 7.95°$) Miller planes of the crystal structure of Ni(OEP). However, the latter two peaks matched the peak positions of the [001] and [010] Miller planes of the reported crystal structure of Pt-(OEP),[23] respectively. Using the solution-phase precipita-tive method, the XRD pattern of the Pt(OEP) nanowires obtained showed two peaks that are similar to those of the other M(OEP) nanowires. We note that the XRD pattern of both Pd(OEP) and Pt(OEP) nanowires are different from the simulated XRD pattern of the reported crystal structure of Pd(OEP)[24] and Pt(OEP),[23] respectively, indicating that both the reported crystal structures of Pd(OEP) and Pt-(OEP) are not suitable for describing the packing of these molecules in the nanowires (see Supporting Information, Figure S1 d and S1 f).

The morphology of the M(OEP) nanowires were exam-ined by TEM (Figure 4) and SEM (see Supporting Informa-tion, Figure S2). The findings revealed that uniform 1D M-(OEP) nanowires were formed by the precipitative method. The diameters for all the M(OEP) nanowires are in the range of 20–70 nm and the monodispersity of the diameters is about 10, revealing that the M(OEP) nanowires are uni-formly assembled (Table 2). The average length of Cu(OEP) nanowires is the shortest (about 150 nm) whilst that of other M(OEP) nanowires range from 480–680 nm. Identification of the metal was confirmed by energy dispersive X-ray
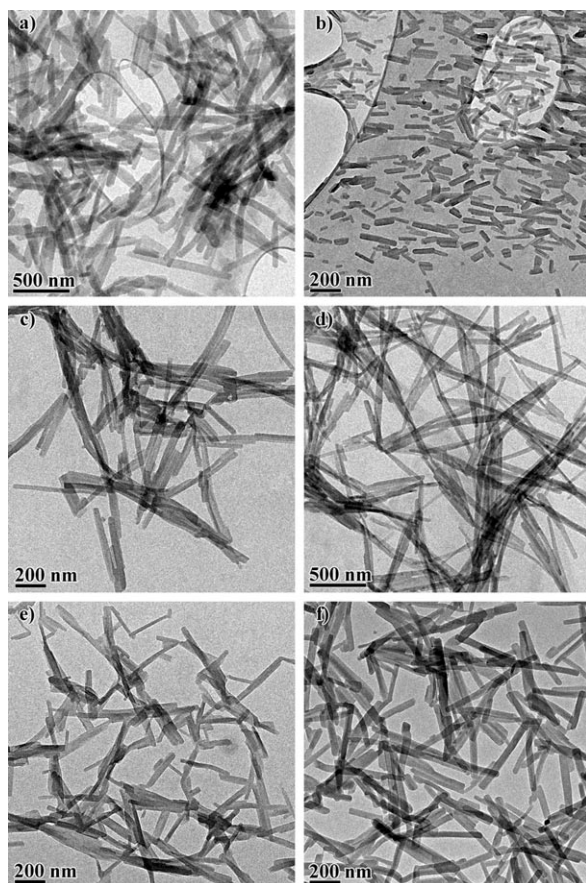
Figure 4. TEM images of a) Ni(OEP); b) Cu(OEP); c) Zn(OEP); d) Pd-(OEP); e) Ag(OEP) and f) Pt(OEP) nanowires fabricated at 10 μM concentration of M(OEP) in 90 % v/v H₂O/tetrahydrofuran.

Table 2. Average diameter and monodispersity of the M(OEP) nanowires prepared at 10 μM concentration of M(OEP) in 90 % (v/v) H₂O/tetrahydrofuran.

M(OEP)	d [nm][a]	Monodispersity [%][b]	l [nm][c]
Ni(OEP)	69.4 ± 8.2	11.8	630 (340–1000)
Cu(OEP)	23.7 ± 2.9	12.2	150 (60–250)
Zn(OEP)	38.4 ± 4.1	10.7	480 (250–600)
Pd(OEP)	42.4 ± 4.4	10.4	680 (390–1020)
Ag(OEP)	27.8 ± 3.8	13.7	600 (250–1100)
Pt(OEP)	41.1 ± 4.6	11.2	570 (230–880)

[a] The average diameter (d) is measured from 300 randomly selected nanowires. [b] Monodispersity of the diameter of nanowires is calculated as follow: monodispersity = (standard deviation/average diameter)x100 %. [c] Owing to the aggregation of nanowires, the average length (l) of the nanowires can only be roughly estimated. Bracketed values indicated the range of the length of the nanowires.

conditions (Figure 5 c–e). Monodispersed spherical Ag-(F₂₀TPP) nanoparticles were obtained, and the average diameter and monodispersity of the nanoparticles were 58.29 ± 6.89 nm and 11.82 %, respectively (Figure 5 c). Ag-(TTP) and Ag(TPP) both assembled into irregular-shaped nanomaterials (Figure 5 d and 5 e, respectively).

To examine the growth direction and crystallinity, SAED analysis was performed on a single M(OEP) nanowire. As depicted in Figure 6, the ordered diffraction spots reveal the single crystallinity of these M(OEP) nanowires. Since the crystal structures of Pd(OEP), Ag(OEP), and Pt(OEP) are similar to that of Ni(OEP), Cu(OEP), or Zn(OEP) as discussed before, the crystal structure data of the latter three complexes were used here to index the diffraction spots and growth direction of the three M(OEP) (M = Pd, Ag, and Pt) nanowires. The growth direction of these M(OEP) nanowires are all along the [001] direction, which is the c-axis of their crystal structures. All the SAED patterns were taken
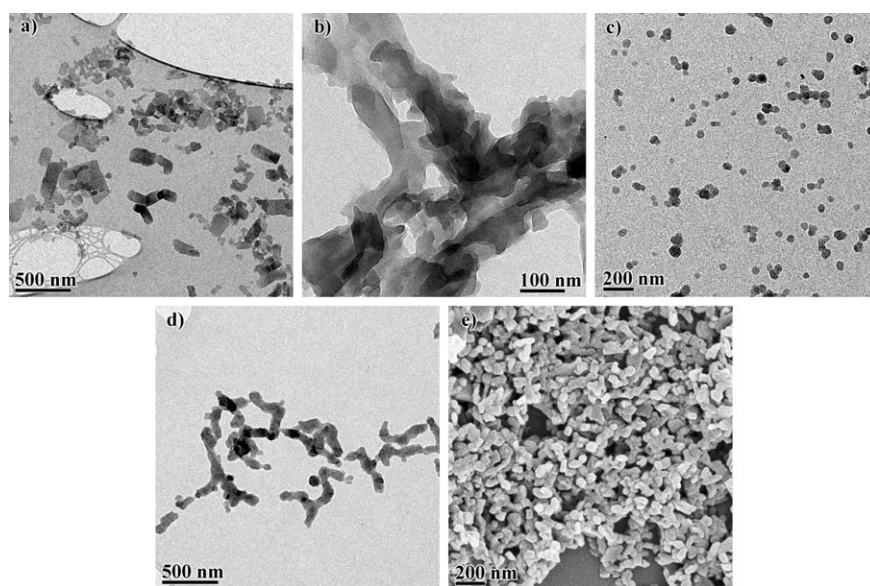
(EDX) microanalysis of the nanowires (see Supporting Information, Figure S3). Examination of the as-synthesized solid sample of M(OEP) showed that the wires were of the micrometer scale (Bulk Ag-(OEP) is illustrated as an example; Supporting Information, Figure S4 a). We have also examined the morphology of free H₂OEP and *meso*-substituted metalloporphyrins prepared by the precipitative method (Figure 5). Free H₂OEP, on the other hand, formed irregular-shaped nanomaterials (Figure 5 a). [Au^III(OEP)]Cl gave irregular-shaped and seriously aggregated materials (Figure 5 b). Three *meso*-substituted Ag(II) porphyrin complexes, namely Ag(F₂₀TPP), Ag(TPP), and Ag-(TTP), were also examined under the same preparation

Figure 5. TEM images of a) H₂OEP nanomaterials; b) [Au^III(OEP)]Cl materials; c) Ag(F₂₀TPP) nanoparticles and d) Ag(TPP) irregular-shaped nanomaterials. e) SEM image of Ag(TTP) irregular-shaped nanomaterials.
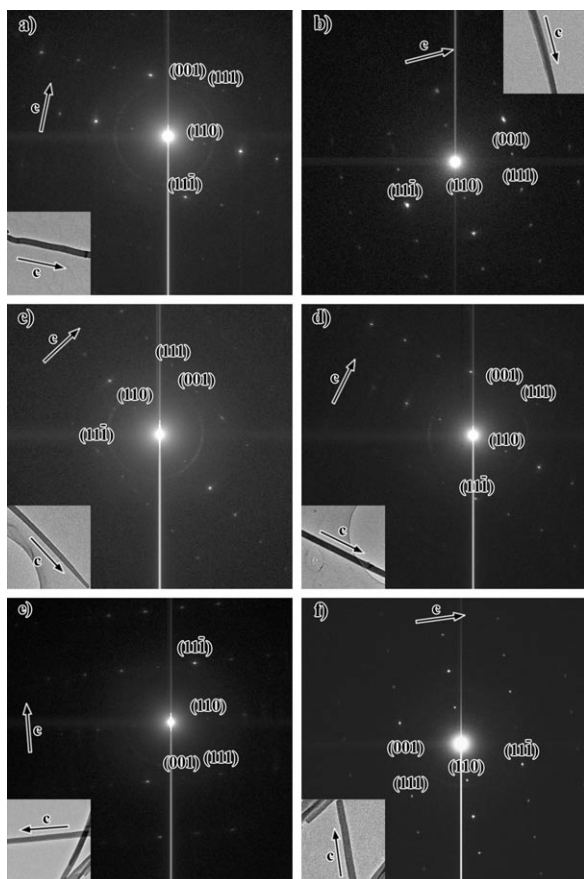
FULL PAPERS

Figure 6. SAED patterns of a) Ni(OEP); b) Cu(OEP); c) Zn(OEP); d) Pd(OEP); e) Ag(OEP) and f) Pt(OEP) nanowire taken at [1-10] zone axis. Insets are the corresponding nanowires.
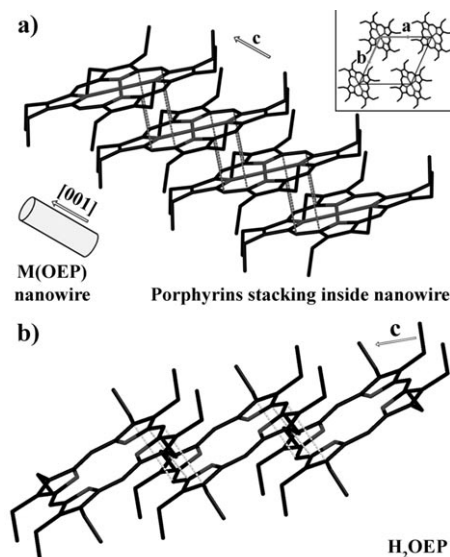

Figure 7. a) View of stacking of porphyrin molecules along c-axis ([001] direction) showing clearly intermolecular π⋯π interaction along c-axis to assemble the nanowires. Broken lines indicate the intermolecular π⋯π interaction. Inset shows the view of the crystal packing arrangement of porphyrin molecules at c-axis. The CIF file of Ni(OEP) triclinic B form crystal is used here as an example to illustrate the packing and self-assembly of M(OEP) porphyrin molecules. b) View of packing of free H_2OEP molecules. Broken lines indicate the intermolecular π⋯π interaction. The CIF file of triclinic H_2OEP is used here. Hydrogen atoms are omitted here for clarity.

at the [1-10] zone axis of the nanowires. The [1-10] Miller plane of the M(OEP) nanowires is normal to the electron beam, consistent with the data that the [1-10] Miller plane shows an intense peak in the powder XRD patterns. As these M(OEP) nanowires preferentially grew along the [001] direction, the peak for the [001] Miller plane is not readily observed in their powder XRD patterns. The [110] Miller plane (diffraction peak at a 2θ value of 12.06°), which is orthogonal to the [1-10] Miller plane, was not intense in the powder XRD patterns and was found parallel to the electron beam. As a result, the M(OEP) nanowires had several dominant [100], [010], and [1-10] Miller planes on their surfaces and only a minor proportion was oriented in the [110] Miller plane. The [001] Miller plane was found to be perpendicular to the plane of the substrate and arranged along the longitudinal axis of the nanowires. We have also examined the crystallinity of the as-synthesized solid sample of M(OEP) (Supporting Information, Figure S4b). Concentric diffraction rings were observed in their SAED patterns, indicative of the polycrystalline nature of these solid samples.

The c-axis of M(OEP) crystals is the direction of stacking of the M(OEP) molecules by intermolecular π⋯π interactions. Self-assembly of molecules along the π⋯π stacking axis to form nanowires has been reported in the literature.[5d,25] Figure 7a depicts the stacking of M(OEP) molecules by intermolecular π⋯π interactions (broken line). The intermolecular π⋯π distance is 3.472 Å, 3.467 Å, and 3.430 Å for Ni(OEP), Cu(OEP), and Zn(OEP), respectively, as determined from their reported crystal structures.[15] The intermolecular π⋯π stacking interactions should be associated with 1D crystal growth of the nanowires. As revealed by its crystal structure, H_2OEP molecules also show intermolecular π⋯π interactions (intermolecular π⋯π distance is 3.494 Å; Figure 7b),[26] but they were found to self-assemble into irregular-shaped nanomaterials only (Figure 5a). This reveals the importance of the metal cation presented in the octaethylporphyrin rings. The M(OEP) molecules obviously show a larger extent of "face-to-face" stacking between the porphyrin rings, owing to the non-covalent dipolar interactions between the metal cation and π-electrons of the porphyrin ring (comparison of Figure 7a with Figure 7b). Viewing along the c-axis signifies the better overlapping of M-(OEP) molecules along the π⋯π stacking axis direction (inset of Figure 7a), consequently leading to a faster crystal growth of the nanowires along the [001] direction. Thus, we reason that no nanowires formed in the Ag(F_{20}TPP), Ag-(TPP), and Ag(TTP) cases because of the steric hindrance of the four *meso*-phenyl substituents that are perpendicular to the porphyrin rings, and consequently the prohibition of the assembly of linear 1D nanowires through intermolecular π⋯π interactions.

Size-controlled synthesis of nanomaterials is a critical step in achieving functional nanomaterials. In this work, Ag-(OEP) was selected to investigate the optimized conditions for the fabrication of M(OEP) nanowires. As depicted in Figure 8, the composition of solvent mixtures is critical in
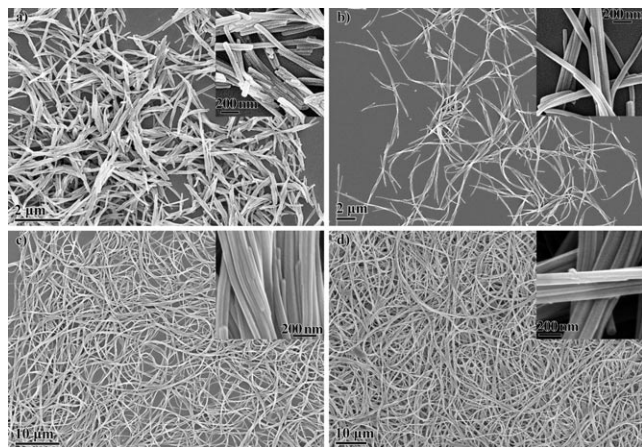

Figure 8. SEM images of the Ag(OEP) nanowires formed at various ratios of H_2O to THF: a) 90%, b) 70%, c) 50% and d) 35% (v/v) H_2O/THF. The concentration of Ag(OEP) is kept at 10 μM. Insets are the SEM images of the same samples at higher magnification.

governing the dimensions of the Ag(OEP) nanowires. The average diameter, monodispersity, and average length of the Ag(OEP) nanowires increase as the ratio of H_2O to tetrahydrofuran (THF) decreases (Table 3 and see also Supporting

Table 3. Average diameter and monodispersity of the Ag(OEP) nanowires prepared at various ratios of H_2O to THF. The concentration of Ag(OEP) was kept at 10 μM.

H_2O/THF [% v/v]	d [nm][a]	Monodispersity [%][b]	l [nm][c]
90	27.8 ± 3.8	13.7	600[d]
70	37.1 ± 5.8	15.6	> 4000
50	47.4 ± 7.8	16.5	> 10000
35	66.5 ± 18.8	28.2	> 10000
30	no nanowires formed		
10	no nanowires formed		

[a] The average diameter (d) is measured from 300 randomly selected nanowires. [b] Monodispersity of the diameter of nanowires is calculated as follow: monodispersity = (standard deviation/average diameter)x100%. [c] Owing to the aggregation of nanowires, the average length (l) of the nanowires is roughly estimated. [d] The range of the length of the nanowires is 250–1100 nm.

Information, Figure S5). Nanowires prepared at lower water content (35% and 50% v/v, H_2O/THF) were dramatically longer (> 10 μm) than those (about 250–4000 nm) prepared at higher water content (70% and 90% v/v, H_2O/THF). The monodispersity of the nanowires obtained was 13.7% at higher water content (90% v/v, H_2O/THF), and 28.2% at lower water content (35% v/v, H_2O/THF), manifesting that the nanowires obtained at higher water content were more

uniform. Also, nanowires fabricated at lower water contents were in larger bundles, containing about 20–30 nanowires (insets of Figure 8). At 10% and 30% (v/v) H_2O/THF, Ag-(OEP) molecules did not give any nanowires.

UV–visible absorption spectroscopy was used to monitor the change of the Soret and Q bands of Ag(OEP) upon formation of nanowires (Figure 9). Upon increasing the water content, the absorbance of the Q bands of the Ag(OEP)
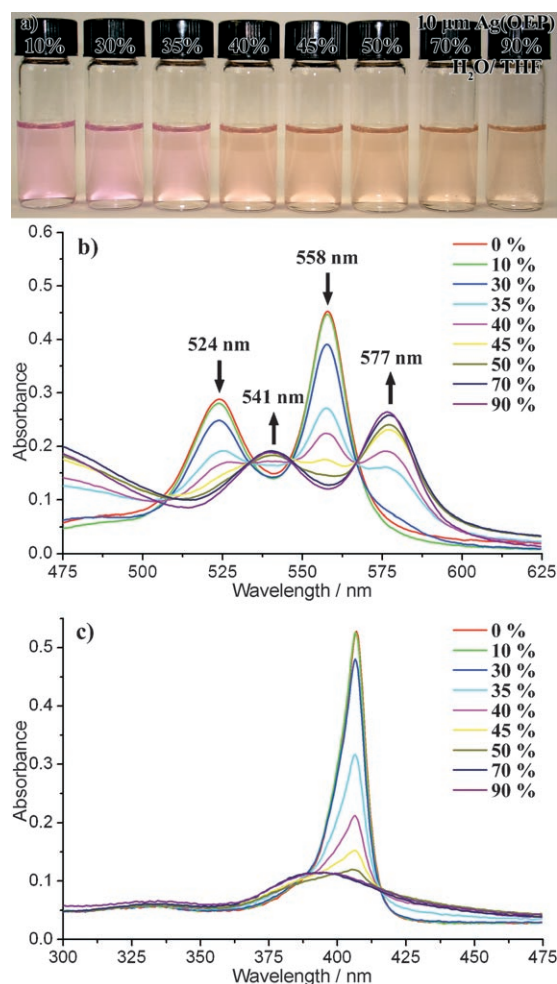

Figure 9. a) Freshly prepared Ag(OEP) nanowires dispersion in 10–90% (v/v) H_2O/THF. b) UV–visible absorption spectra showing the Q band region of Ag(OEP) nanowires fabricated at 10–90% (v/v) H_2O/THF recorded with a 1 cm quartz cuvette. c) UV–visible absorption spectra showing the Soret band region of the same Ag(OEP) nanowires sample recorded with a 1 mm quartz cuvette.

molecule at 524 and 558 nm decreases. The peak absorbances at 541 and 577 nm, attributed to the aggregation of Ag-(OEP) molecules, increase upon changing the composition of the H_2O/THF mixture from 35% to 90% (v/v), consistent with the TEM data that Ag(OEP) nanowires started to form under these conditions. The λ_{max} of the Q bands red-shifts upon aggregation of Ag(OEP) molecules to form nanowires. The intensity of the Soret band of Ag(OEP) mol-

FULL PAPERS

ecule at 406 nm decreases and eventually flattens upon aggregation of the molecules.

Size control of M(OEP) nanowires, by changing the ratio of H_2O to THF, can be understood by considering the steps of nucleation and growth in the course of the precipitative method, as depicted in Figure 10. M(OEP) was firstly dis-
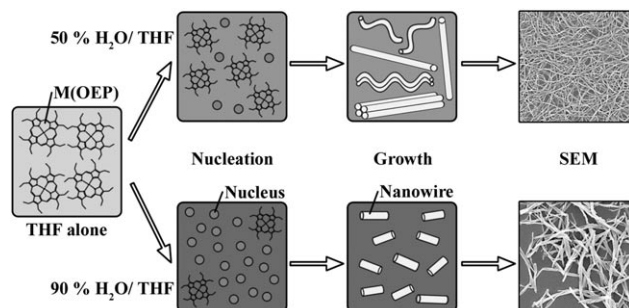

Figure 10. Schematic diagram illustrating the effect of different composition of H_2O (poor solvent) to THF (good solvent) on the self-assembly of M(OEP) nanowires.

solved in a "good" solvent (THF). A "poor" solvent (H_2O) was added to induce formation of nuclei. At high water content (90% v/v, H_2O/THF), a fast nucleation step resulted and most of the dissolved M(OEP) molecules were precipitated to form nuclei. The thickness of the nanowires became uniform. In the growth step, the remaining M(OEP) molecules would assemble and grow on the nuclei. Ostwald ripening might also take place to consume small nuclei or crystals for growth.[27] Owing to the anisotropic nature of the intermolecular interactions between M(OEP) molecules, one dimensional linear nanowires were obtained. Since only a small number of M(OEP) molecules remained, the nanowires fabricated were shorter. At low water content (50% v/v, H_2O/THF), as less H_2O was added, the nucleation rate was reduced, resulting in a wider distribution of the thickness of nanowires. Since most of the M(OEP) molecules did not precipitate out, more molecules were available for assembly into longer nanowires.

We have also examined the effect of the M(OEP) concentration on the size of nanowires (see Supporting Information, Figure S6). At 20 μM concentration of Ag(OEP) (90% v/v, H_2O/THF), the average diameter and monodispersity of the Ag(OEP) nanowires were 27.9 ± 3.3 nm and 11.8%, respectively. The average length of the nanowires was about 400 nm. This result is similar to the Ag(OEP) nanowires fabricated at 10 μM concentration of Ag(OEP). However, at higher Ag(OEP) concentrations of 50 or 100 μM (90% v/v, H_2O/THF), the size of the Ag(OEP) wires increased from the nanometer to the micrometer scale (> 1 μm) and the diameters were not uniform. Presumably, a large amount of nuclei were formed, owing to the high Ag(OEP) concentration. These nuclei and small crystals could easily aggregate together and grow into large micrometer-scale crystals.

We have also studied the effect of the solvent system on the fabrication of nanowires (see Supporting Information, Figure S7). $CHCl_3$ is a "good" solvent while methanol (MeOH) is a "poor" solvent for Ag(OEP). Ag(OEP) nanowires fabricated at 95% (v/v) MeOH/$CHCl_3$ (10 μM concentration of Ag(OEP)) were shorter (about 4–5 μm) and the average diameter of the nanowires was about 200 nm. Those fabricated at 90% (v/v) MeOH/$CHCl_3$ were much longer (> 10 μm) and the average diameter of the nanowires was about 500 nm. In 10–80% (v/v) MeOH/$CHCl_3$, no crystalline sample of Ag(OEP) was found. Compared to those prepared in H_2O/THF, the nanowires formed in MeOH/$CHCl_3$ were generally not uniform and larger.

We used bottom contact field effect transistor structure as a tool to analyze the charge transporting properties of the M(OEP) nanowires fabricated at 10 μM concentration of M-(OEP) in 90% (v/v) H_2O/THF solution mixture. A suspension of M(OEP) nanowires was drop cast on the top of a lithographically patterned bottom contact field effect transistor (FET) structure (Figure 11). These M(OEP) nano-
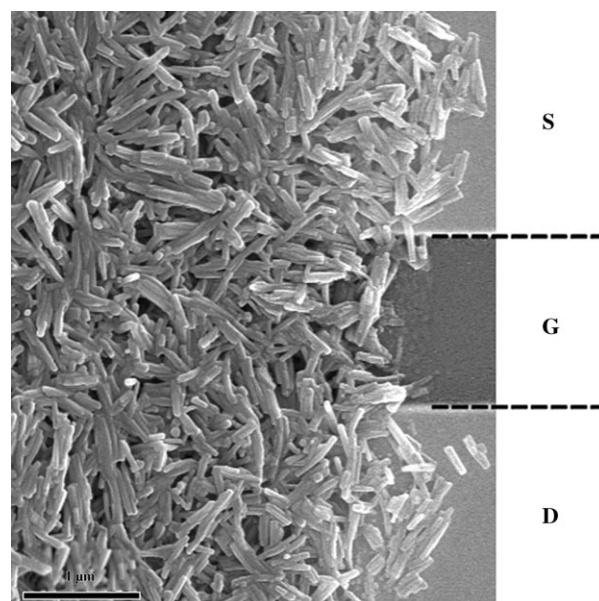

Figure 11. SEM image of the surface of a bottom-contact device with M-(OEP) nanowires connecting the source (**S**) and drain (**D**) electrodes.

wires, which aggregated together forming a film connecting the source and drain electrodes, exhibited a clear gate modulation on the channel current for different gate bias, as depicted in Figure 12 (see also Supporting Information, Figure S8). The drain-source current I_{DS} negatively increased with negative gate voltages of V_G indicative of a p-type field effect transistor behavior. However, the channel was open even at $V_G = 0$ V probably arising from the bulk conduction or parallel conduction caused by the aggregation of nanowires between source and drain electrodes. Although an ideal field effect transistor behaviour with a closed channel at zero gate voltage was not found for these FET devices, a
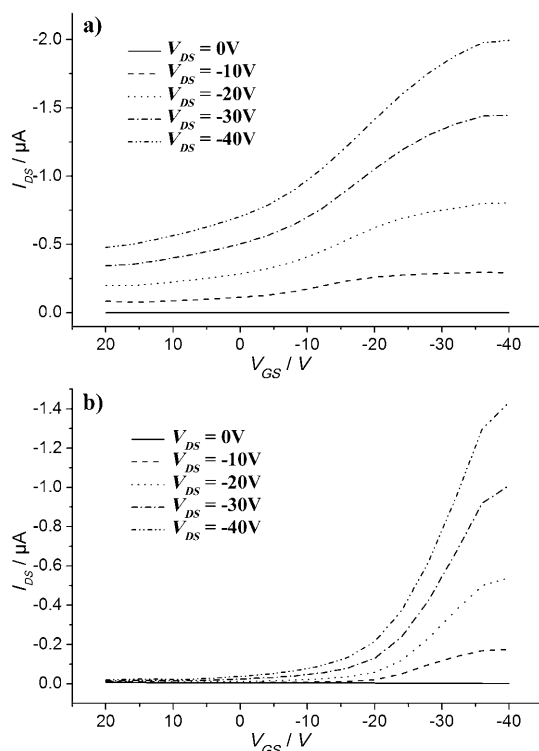
Figure 12. Transfer characteristics of devices that consist of a) Ag(OEP) and b) Ni(OEP) nanowires at different drain-source voltages.

clear gate modulation on the drain current has been observed.[28] In this regard, a simple FET analysis can be used to evaluate the charge mobility. Since a saturation of the drain current was not attained, the charge-carrier mobility (μ, $cm^2 V^{-1} s^{-1}$) was calculated in the linear regime (where $V_{DS} \ll V_{GS}$) using the $I_{D,lin}$ versus V_G relation. The results are summarized in Table 4.[29] The charge-carrier mobility of all

Table 4. Charge-carrier mobility of different M(OEP) nanowires fabricated at 10 μM concentration of M(OEP) in 90% (v/v) H_2O/THF.

M(OEP)	Charge-carrier mobility [$cm^2 V^{-1} s^{-1}$]
H_2OEP	3.0×10^{-5}
Ni(OEP)	6.0×10^{-2}
Cu(OEP)	4.2×10^{-3}
Zn(OEP)	2.1×10^{-2}
Pd(OEP)	1.2×10^{-3}
Ag(OEP)	6.6×10^{-2}
Pt(OEP)	1.6×10^{-3}

M(OEP) nanowires are about 10^{-3}–10^{-2} $cm^2 V^{-1} s^{-1}$, which are at least two orders of magnitude higher than that of H_2OEP nanomaterials (10^{-5} $cm^2 V^{-1} s^{-1}$). We attribute this large discrepancy in charge-carrier mobility to the larger extent of face-to-face stacking of M(OEP) molecules, resulting in better overlapping of M(OEP) molecules and higher charge-carrier mobility,[30] as a consequence of the presence of an M^{2+} ion in the porphyrinato ring. We have fabricated and characterized devices with Ag(F_{20}TPP), Ag(TPP), and

Ag(TTP) nanomaterials, all of which did not exhibit field effect transistor performance. These three *meso*-substituted porphyrins have bulky phenyl substituents, and hence intermolecular π···π interactions are prohibited. Owing to their good crystallinity, the M(OEP) nanowires exhibited charge mobility an order of magnitude higher than the vacuum-deposited M(OEP) thin films.[16c]

Conclusions

We have successfully demonstrated the fabrication of uniform M(OEP) (M=Ni, Cu, Zn, Pd, Ag, and Pt) nanowires with well-defined size and shape by a simple, surfactant-free, and solution-phase precipitative method. The narrow distribution of the diameters of M(OEP) nanowires reveals uniform assembly of the nanowires. The size of the M(OEP) nanowires can be controlled by changing the composition of solvent mixtures. Previous works on porphyrin nanowires made use of UV–visible spectrophotometry for the characterization revealing that the porphyrin molecules self-assemble together by J-aggregation or ionic interaction. In this work, we characterized the nanowires by XRD and SAED techniques, and have provided evidence that the nanowires grow along the π···π stacking direction of M(OEP) molecules. The better stacking of M(OEP) molecules results from the electrostatic interaction between the metal cation and π-electrons of the porphyrin ring, leading to an anisotropic growth of nanowires. The M(OEP) nanowires exhibited a charge-carrier mobility of 10^{-3}-10^{-2} $cm^2 V^{-1} s^{-1}$, which are at least two orders of magnitude higher than that of H_2OEP. The charge-carrier mobility of the devices based on M(OEP) nanowires are an order of magnitude higher than the vacuum-deposited M(OEP) thin films.

Experimental Section

Chemicals

All the chemicals were analytical reagent grade, and were used as received without further purification except otherwise noted. 5,10,15,20-tetrakis(pentafluorophenyl)porphyrin (H_2F_{20}TPP, Frontier Scientific), 2,3,7,8,12,13,17,18-octaethylporphyrin (H_2OEP, Frontier Scientific), 2,3,7,8,12,13,17,18-octaethylporphyrin nickel(II) (Ni(OEP), Aldrich, 97%), 2,3,7,8,12,13,17,18-octaethylporphyrin copper(II) (Cu(OEP), Aldrich), 2,3,7,8,12,13,17,18-octaethylporphyrin palladium(II) (Pd(OEP), Aldrich), $AgNO_3$, (Aldrich, >99.0%), $Zn(CH_3COO)_2 \cdot 2H_2O$ (Aldrich, >98%), $PtCl_2$ (Aldrich, 98%), $KAuCl_4$ (Oxkem Limited) were purchased from commerical sources and used without further purification. Tetrahydrofuran (THF) was purchased from TEDIA and purified by PURESOLV solvent purification systems from Innovative Technology Inc. *meso*-Tetraphenylporphyrin (H_2TPP),[31] *meso*-tetrakis(4-tolyl)porphyrin (H_2TTP),[31] Ag(Por) (Por=TPP, TTP and OEP dianions),[26] Zn-(OEP),[15c] Pt(OEP),[21] and [Au^{III}(OEP)]Cl,[22] were synthesized and characterized by the literature methods.

Instrumentation

Nanowires were characterized by powder X-ray diffraction (XRD), transmission electron microscope (TEM), selected area electron diffraction (SAED) analysis, energy-dispersive X-ray microanalysis (EDX), scanning

electron microscope (SEM), and ultraviolet–visible spectroscopy (UV/Vis). The powder XRD measurements were performed on a Bruker D8 ADVANCE X-ray diffractometer with parallel Cu K$_{\alpha}$ radiation ($\lambda = 1.5406$ Å). The scanning rate is 0.005°/s in the 2θ range from 5 to 30° and the step size is 0.05°. The XRD samples were prepared by either dropping a freshly prepared dispersion of M(OEP) nanowires onto silicon wafer substrates or placing recrystallized solid samples onto glass slides. Powder XRD simulation was performed by Mercury version 1.4,[32] using those atomic coordinates from the reported CIF files. The simulation wavelength was set at 1.5406 Å. The 2θ range was from 5 to 30° and step was 0.05°. The peak full width at half maximum (FWHM) was set at 0.1°. TEM and SAED analysis were done on Philips Tecnai G2 20 S-TWIN with an accelerating voltage of 200 kV. The TEM images were taken by Gatan MultiScan Camera Model 794. The EDX analysis was performed on Oxford Instruments Inca with a scanning range from 0 to 20 keV. The SEM images were taken on LEO 1530 FEG operating at 5 kV. The TEM samples were prepared by dropping a drop of the suspension of freshly prepared M(OEP) nanowires on the formvar-coated copper grids and then dried in a vacuum desiccator. The SEM samples were prepared by dropping the suspension of freshly prepared M(OEP) nanowires onto silicon wafers. The SEM samples were coated with a thin layer of gold by sputter coater. UV/Vis absorption measurements were recorded on a Perkin–Elmer Lambda 900 UV–visible spectrophotometer. ^{1}H NMR spectra were recorded on Bruker DPX-300 or Avance400 FT-NMR spectrometers with chemical shifts (in ppm) relative to tetramethylsilane. Positive ion mass spectra were recorded on a matrix-assisted laser desorption/ionization mass spectrometer (Voyager-DE STR, Applied Biosystems, USA) equipped with a N$_2$ laser (337 nm).

Single-Crystal X-ray Diffraction: Crystals of Ag(F$_{20}$TPP) were obtained by slow evaporation of a n-hexane solution of Ag(F$_{20}$TPP). A purple crystal having dimensions of $0.4 \times 0.3 \times 0.15$ mm mounted in a glass capillary was used for data collection at 28°C on a Bruker Smart CCD 1000 using graphite monochromatized Mo-K$_{\alpha}$ radiation ($\lambda = 0.71073$ Å). The structure was solved by direct method employing SHELXS-97 program on PC.[33] Ag and many non-H atoms were readily located at the beginning. The positions of the other non-hydrogen atoms were found after successful refinement by full-matrix least-squares using program SHELXL-97. CCDC 682925 contains the supplementary crystallographic data for this paper. These data can be obtained free of charge from The Cambridge Crystallographic Data Centre at www.ccdc.cam.ac.uk/data_request/cif.

Synthesis

Ag(F$_{20}$TPP): Acetic acid (20 mL) was first degassed with argon for 30 min. Degassed acetic acid was heated to reflux at 120°C under an argon atmosphere. H$_2$F$_{20}$TPP (94 μmol), AgNO$_3$ (0.94 mmol), and CH$_3$COONa (1 mmol) were added to the refluxing acetic acid. The solution mixture was refluxed for an hour under an argon atmosphere. The metalation was monitored by the disappearance of the Q band using UV–Visible spectrophotometry. The mixture was cooled to room temperature and transferred to a separating funnel. CH$_2$Cl$_2$ (50 mL) was used to extract the product. The CH$_2$Cl$_2$ layer was washed with water (3×50 mL) and subsequently with saturated Na$_2$CO$_3$ solution (3×50 mL) to remove acetic acid, AgNO$_3$, and CH$_3$COONa. CH$_2$Cl$_2$ solvent was removed under reduced pressure and the solid was dried under vacuum. The solid was dissolved in CHCl$_3$ (3 mL) and purified by column chromatography on a neutral 90-alumina using CH$_2$Cl$_2$/n-hexane (3% v/v) as eluent. Ag-(F$_{20}$TPP) was eluted out at the first red band. Upon removal of solvent, a reddish–purple solid was obtained. Successful crystal growth was attained by slow evaporation of an n-hexane solution of Ag(F$_{20}$TPP). The crystals obtained were cubic purple crystals. Yield 40%; UV/Vis (CHCl$_3$): λ_{max} (log ε) = 419 (5.62), 499 (3.56), 537 (4.29), 569 nm (3.82); MS (MALDI-TOF): $m/z = 1081$ [M^+]; elemental analysis: calcd (%) for C$_{44}$H$_8$N$_4$F$_{20}$Ag$_1$: C 48.92, H 0.75, N 5.19; found: C 48.77, H 0.74, N 5.13.

Ag(TPP): Yield 70%; UV/Vis (CHCl$_3$): λ_{max} (log ε) = 426 (5.48), 506 (3.51), 541 (4.10), 574 nm (3.48); MS (MALDI-TOF): $m/z = 721$ [M^+]; elemental analysis: calcd (%) for C$_{44}$H$_{28}$N$_4$Ag$_1$: C 73.34, H 3.92, N 7.78; found: C 73.21, H 3.90, N 7.58.

Ag(TTP): Yield 67%; UV/Vis (CHCl$_3$): λ_{max} (log ε) = 427 (5.51), 507 (3.54), 542 (4.14), 576 nm (3.59); MS (MALDI-TOF): $m/z = 777$ [M^+]; elemental analysis: calcd (%) for C$_{48}$H$_{36}$N$_4$Ag$_1$: C 74.23, H 4.67, N 7.21; found: C 74.06, H 4.63, N 7.05.

Ag(OEP): Yield 60%; UV/Vis (CHCl$_3$): λ_{max} (log ε) = 408 (5.50), 525 (4.18), 559 nm (4.34); MS (MALDI-TOF): $m/z = 641$ [M^+]; elemental analysis: calcd (%) for C$_{36}$H$_{44}$N$_4$Ag$_1$: C 67.49, H 6.92, N 8.75; found: C 67.25, H 6.91, N 8.53.

Zn(OEP): Yield 50%; ^{1}H NMR (400 MHz, CDCl$_3$, 25°C, TMS): $\delta = 1.95$ (t, ^{3}J(H,H) = 7.53 Hz, 24H; CH$_3$), 4.14 (q, ^{3}J(H,H) = 7.55 Hz, 16H; CH$_2$), 10.18 ppm (s, 4H; *meso*-CH); UV/Vis (CHCl$_3$): λ_{max} (log ε): 402 (5.46), 533 (4.14), 569 nm (4.28); MS (MALDI-TOF): $m/z = 596$ [M^+]; elemental analysis: calcd (%) for C$_{36}$H$_{44}$N$_4$Zn$_1$: C 72.29, H 7.41, N 9.37; found: C 71.16, H 7.33, N 9.06.

Pt(OEP): Yield 75%; ^{1}H NMR (300 MHz, CDCl$_3$, 25°C, TMS): $\delta = 1.90$ (t, ^{3}J(H,H) = 7.57 Hz, 24H; CH$_3$), 4.02 (q, ^{3}J(H,H) = 7.55 Hz, 16H; CH$_2$), 10.02 ppm (s, 4H; *meso*-CH); UV/Vis (CHCl$_3$): λ_{max} (log ε) = 381 (5.50), 501 (4.15), 535 nm (4.79); MS (MALDI-TOF): $m/z = 727$ [M^+]; elemental analysis: calcd (%) for C$_{36}$H$_{44}$N$_4$Pt$_1$: C 59.41, H 6.09, N 7.70; found: C 59.32, H 6.01, N 7.54.

[Au^{III}(OEP)]Cl: Yield 43%; ^{1}H NMR (300 MHz, CDCl$_3$, 25°C, TMS): $\delta = 2.01$ (t, ^{3}J(H,H) = 7.38 Hz, 24H; CH$_3$), 4.29 (q, ^{3}J(H,H) = 7.48 Hz, 16H; CH$_2$), 10.76 ppm (s, 4H; *meso*-CH); UV/Vis (CHCl$_3$): λ_{max} (log ε) = 389 (5.28), 510 (3.85), 546 nm (4.13); MS (MALDI-TOF): $m/z = 729$ [M^+]; elemental analysis: calcd (%) for C$_{36}$H$_{44}$N$_4$ClAu$_1$: C 56.51, H 5.80, N 7.32; found: C 56.10, H 5.65, N 7.12.

M(OEP) Nanowires: The precipitative method was adopted to synthesize the M(OEP) nanowires.[7f–g] Generally, a THF solution containing M-(OEP) (100 μM, 1 mL) was injected to H$_2$O (9 mL) at once to give an orange suspension of nanowires. The nanowires were collected by centrifugation and stored for further characterizations. To optimize the conditions for the preparation of M(OEP) nanowires, Ag(OEP) was chosen to examine the effect of a different composition of solvent mixtures and concentration on the formation of M(OEP) nanowires.

Field Effect Charge-carrier Mobility Measurement

A gate oxide SiO$_2$ layer (100 nm, relative permittivity = 3.9) was thermally grown on n-type Si substrates (the gate electrode). Image reversal photolithography followed by a standard lift-off process was done for the Ti/Au source/drain contact patterns. The fabricated devices have a channel length of 1.5 to 5 μm and a width of 400 to 1048 μm. A suspension of M-(OEP) nanowires was drop cast on the top of the bottom contact devices and dried inside the glove box. The fabricated devices were characterized inside an Mbraun nitrogen glove box (oxygen and water level were kept less than 0.1 ppm) by a probe-station using a Keithley semiconductor parameter analyzer, K4200. Since saturation of the drain current was not attained, the charge-carrier mobility (μ) was calculated in the linear regime using the equation below (where $V_{DS} \ll V_{GS}$)[28],

$$\mu = \frac{L}{WC_{ox}V_{DS}}\frac{\partial I_{DS}}{\partial V_{GS}} \tag{1}$$

where W is the channel width; L is the channel length; C_{ox} is the capacitance of the SiO$_2$ insulating layer; V_{GS} is the gate voltage; V_{DS} is the drain-source potential and I_{DS} is the channel (drain-source) current.

[1] For general reviews, see: a) C. Burda, X. Chen, R. Narayanan, M. A. El-Sayed, *Chem. Rev.* **2005**, *105*, 1025–1102, and references therein; b) *The Chemistry of Nanomaterials: Synthesis Properties and Applications*, Vol. 1 & 2 (Eds.: C. N. R. Rao, A. Muller, A. K. Cheetham), Wiley-VCH, Weinheim **2004**.

[2] a) J. Hu, T. W. Odom, C. M. Lieber, *Acc. Chem. Res.* **1999**, *32*, 435–445; b) Y. Xia, P. Yang, Y. G. Sun, Y. Y. Wu, B. Mayer, B. Gates, Y. Yin, F. Kim, H. Yan, *Adv. Mater.* **2003**, *15*, 353–389; c) M. Law, J. Goldberger, P. Yang, *Annu. Rev. Mater. Res.* **2004**, *34*, 83–122; d) A. P. H. J. Schenning, E. W. Meijer, *Chem. Commun.* **2005**, 3245–3258; e) Y. Li, F. Qian, J. Xiang, C. M. Lieber, *Mater. Today* **2006**, *9*, 18–27; f) W. Lu, C. M. Lieber, *Nat. Mater.* **2007**, *6*, 841–850; g) A. Facchetti, *Mater. Today* **2007**, *10*, 28–37.

[3] a) A. de la Escosura, M. V. Martinez-Diaz, P. Thordarson, A. E. Rowan, R. J. M. Nolte, T. Torres, *J. Am. Chem. Soc.* **2003**, *125*, 12300–12308; b) F. Yang, M. Shtein, S. R. Forrest, *Nat. Mater.* **2005**, *4*, 37–41; c) Q. Tang, H. Li, M. He, W. Hu, C. Liu, K. Chen, C. Wang, Y. Liu, D. Zhu, *Adv. Mater.* **2006**, *18*, 65–68; d) W. Y. Tong, A. B. Djurišić, M. H. Xie, A. C. M. Ng, K. Y. Cheung, W. K. Chan, Y. H. Leung, H. W. Lin, S. Gwo, *J. Phys. Chem. B* **2006**, *110*, 17406–17413.

[4] a) L. Schmidt-Mende, A. Fechtenkötter, K. Müllen, E. Moons, R. H. Friend, J. D. MacKenzie, *Science* **2001**, *293*, 1119–1122; b) A. P. H. J. Schenning, J. v. Herrikhuyzen, P. Jonkheijm, Z. Chen, F. Würthner, E. W. Meijer, *J. Am. Chem. Soc.* **2002**, *124*, 10252–10253; c) K. Sugiyasu, N. Fujita, S. Shinkai, *Angew. Chem.* **2004**, *116*, 1249–1253; *Angew. Chem. Int. Ed.* **2004**, *43*, 1229–1233; d) F. Würthner, Z. Chen, F. J. M. Hoeben, P. Osswald, C.-C. You, P. Jonkheijm, J. v. Herrikhuyzen, A. P. H. J. Schenning, P. P. A. M. van der Schoot, E. W. Meijer, E. H. A. Beckers, S. C. J. Meskers, R. A. J. Janssen, *J. Am. Chem. Soc.* **2004**, *126*, 10611–10618; e) J. Hernando, P. A. J. de Witte, E. M. H. P. van Dijk, J. Korterik, R. J. M. Nolte, A. E. Rowan, M. F. García-Parajó, N. F. van Hulst, *Angew. Chem.* **2004**, *116*, 4137–4141; *Angew. Chem. Int. Ed.* **2004**, *43*, 4045–4049; f) A. Datar, K. Balakrishnan, X. Yang, X. Zuo, J. Huang, R. Oitker, M. Yen, J. Zhao, D. M. Tiede, L. Zang, *J. Phys. Chem. B* **2006**, *110*, 12327–12332; g) L. Kang, Z. Wang, Z. Cao, Y. Ma, H. Fu, J. Yao, *J. Am. Chem. Soc.* **2007**, *129*, 7305–7312.

[5] a) H. Liu, Y. Li, S. Xiao, H. Gan, T. Jiu, H. Li, L. Jiang, D. Zhu, D. Yu, B. Xiang, Y. Chen, *J. Am. Chem. Soc.* **2003**, *125*, 10794–10795; b) Y. Sakamoto, T. Suzuki, M. Kobayashi, Y. Gao, Y. Fukai, Y. Inoue, F. Sato, S. Tokito, *J. Am. Chem. Soc.* **2004**, *126*, 8138–8140; c) X. Zhang, X. Zhang, W. Shi, X. Meng, C. Lee, S. Lee, *J. Phys. Chem. B* **2005**, *109*, 18777–18780; d) A. L. Briseno, S. C. B. Mannsfeld, X. Lu, Y. Xiong, S. A. Jenekhe, Z. Bao, Y. Xia, *Nano Lett.* **2007**, *7*, 668–675; e) C. Barrett, D. Iacopino, D. O'Carroll, G. De Marzi, D. A. Tanner, A. J. Quinn, G. Redmond, *Chem. Mater.* **2007**, *19*, 338–340.

[6] a) Y. Sun, K. Ye, H. Zhang, J. Zhang, L. Zhao, B. Li, G. Yang, B. Yang, Y. Wang, S.-W. Lai, C.-M. Che, *Angew. Chem.* **2006**, *118*, 5738–5741; *Angew. Chem. Int. Ed.* **2006**, *45*, 5610–5613; b) W. Lu, V. A. L. Roy, C.-M. Che, *Chem. Commun.* **2006**, 3972–3974; c) W. Lu, S.-Y. Chui, K.-M. Ng, C.-M. Che, *Angew. Chem. Int. Ed.* **2008**, *47*, 4568–4572; *Angew. Chem.* **2008**, *120*, 4644–4648.

[7] For reviews, see: a) J.-C. Chambron, V. Heitz, J.-P. Sauvage, in *The Porphyrin Handbook*, Vol. 6 (Eds.: K. M. Kadish, K. M. Smith, R. Guilard), Academic Press, New York **2000**, pp. 1–42; b) J.-H. Chou, M. E. Kosal, H. S. Nalwa, N. A. Rakow, K. S. Suslick, in *The Porphyrin Handbook*, Vol. 6 (Eds.: K. M. Kadish, K. M. Smith, R. Guilard), Academic Press, New York **2000**, pp. 43–131.

[8] X. Gong, T. Milic, C. Xu, J. D. Batteas, C. M. Drain, *J. Am. Chem. Soc.* **2002**, *124*, 14290–14291.

[9] a) A. D. Schwab, D. E. Smith, C. S. Rich, E. R. Young, W. F. Smith, J. C. de Paula, *J. Phys. Chem. B* **2003**, *107*, 11339–11345; b) A. D. Schwab, D. E. Smith, B. Bond-Watts, D. E. Johnston, J. Hone, A. T. Johnson, J. C. de Paula, W. F. Smith, *Nano Lett.* **2004**, *4*, 1261–1265; c) S. C. Doan, S. Shanmugham, D. E. Aston, J. L. McHale, *J. Am. Chem. Soc.* **2005**, *127*, 5885–5892; d) L. M. Scolaro, A. Romeo, M. A. Castriciano, N. Micali, *Chem. Commun.* **2005**, 3018–3020.

[10] a) Z. Wang, C. J. Medforth, J. A. Shelnutt, *J. Am. Chem. Soc.* **2004**, *126*, 15954–15955; b) Z. Wang, C. J. Medforth, J. A. Shelnutt, *J. Am. Chem. Soc.* **2004**, *126*, 16720–16721; c) J.-S. Hu, Y.-G. Guo, H.-P. Liang, L.-J. Wan, L. Jiang, *J. Am. Chem. Soc.* **2005**, *127*, 17090–17095; d) T. Kojima, R. Harada, T. Nakanishi, K. Kaneko, S. Fukuzumi, *Chem. Mater.* **2007**, *19*, 51–58.

[11] a) A. P. H. J. Schenning, F. B. G. Benneker, H. P. M. Geurts, X. Y. Liu, R. J. M. Nolte, *J. Am. Chem. Soc.* **1996**, *118*, 8549–8552; b) H. A. M. Biemans, A. E. Rowan, A. Verhoeven, P. Vanoppen, L. Latterini, J. Foekema, A. P. H. J. Schenning, E. W. Meijer, F. C. de Schryver, R. J. M. Nolte, *J. Am. Chem. Soc.* **1998**, *120*, 11054–11060; c) C. R. L. P. N. Jeukens, M. C. Lensen, F. J. P. Wijnen, J. A. A. W. Elemans, P. C. M. Christianen, A. E. Rowan, J. W. Gerritsen, R. J. M. Nolte, J. C. Maan, *Nano Lett.* **2004**, *4*, 1401–1406; d) M. C. Lensen, K. Takazawa, J. A. A. W. Elemans, C. R. L. P. N. Jeukens, P. C. M. Christianen, J. C. Maan, A. E. Rowan, R. J. M. Nolte, *Chem. Eur. J.* **2004**, *10*, 831–839.

[12] Z. Wang, Z. Li, C. J. Medforth, J. A. Shelnutt, *J. Am. Chem. Soc.* **2007**, *129*, 2440–2441.

[13] a) R. Rotomskis, R. Augulis, V. Snitka, R. Valiokas, B. Liedberg, *J. Phys. Chem. B* **2004**, *108*, 2833–2838; b) M. A. Castriciano, A. Romeo, V. Villari, N. Micali, L. M. Scolaro, *J. Phys. Chem. B* **2004**, *108*, 9054–9059.

[14] J. A. A. W. Elemans, R. van Hameren, R. J. M. Nolte, A. E. Rowan, *Adv. Mater.* **2006**, *18*, 1251–1266.

[15] a) T. D. Brennan, W. R. Scheidt, J. A. Shelnutt, *J. Am. Chem. Soc.* **1988**, *110*, 3919–3924; b) R. Pak, W. R. Scheidt, *Acta Crystallogr. C* **1991**, *47*, 431–433; c) A. Ozarowski, H. M. Lee, A. L. Balch, *J. Am. Chem. Soc.* **2003**, *125*, 12606–12614.

[16] a) Y.-Y. Noh, J.-J. Kim, Y. Yoshida, K. Yase, *Adv. Mater.* **2003**, *15*, 699–702; b) Y.-Y. Noh, J.-J. Kim, K. Yase, S. Nagamatsu, *Appl. Phys. Lett.* **2003**, *83*, 1243–1245; c) C.-M. Che, H.-F. Xiang, S. S.-Y. Chui, Z.-X. Xu, V. A. L. Roy, J. J. Yan, W.-F. Fu, P. T. Lai, I. D. Williams, *Chem. Asian J.* **2008**, *3*, 1092–1103.

[17] M. A. Baldo, D. F. O'Brien, Y. You, A. Shoustikov, S. Sibley, M. E. Thompson, S. R. Forrest, *Nature* **1998**, *395*, 151–154.

[18] Y. Shao, Y. Yang, *Adv. Mater.* **2005**, *17*, 2841–2844.

[19] P. O'Brien, N. Pickett, in *The Chemistry of Nanomaterials: Synthesis Properties and Applications*, Vol. 1 (Eds.: C. N. R. Rao, A. Muller, A. K. Cheetham), Wiley-VCH, Weinheim, **2004**, pp. 12–30.

[20] G. M. Godziela, H. M. Goff, *J. Am. Chem. Soc.* **1986**, *108*, 2237–2243.

[21] J. W. Buchler, L. Puppe, *Liebigs Ann. Chem.* **1974**, 1046–1062.

[22] a) E. B. Fleischer, A. Laszlo, *Inorg. Nucl. Chem. Lett.* **1969**, *5*, 373–376; b) C.-M. Che, R. W.-Y. Sun, W.-Y. Yu, C.-B. Ko, N. Zhu, H. Sun, *Chem. Commun.* **2003**, 1718–1719; c) R. W. Y. Sun, Ph. D. thesis, The University of Hong Kong, Hong Kong SAR, China, **2004**; d) Y. Wang, Q.-Y. He, R. W.-Y. Sun, C.-M. Che, J.-F. Chiu, *Cancer Res.* **2005**, *65*, 11553–11564.

[23] L. R. Milgrom, R. N. Sheppard, A. M. Z. Slawin, D. J. Williams, *Polyhedron* **1988**, *7*, 57–61.

[24] A. M. Stolzenberg, L. J. Schussel, J. S. Summers, B. M. Foxman, J. L. Petersen, *Inorg. Chem.* **1992**, *31*, 1678–1686.

[25] K. Balakrishnan, A. Datar, R. Oitker, H. Chen, J. Zuo, L. Zang, *J. Am. Chem. Soc.* **2005**, *127*, 10496–10497.

[26] J. W. Lauher, J. A. Ibers, *J. Am. Chem. Soc.* **1973**, *95*, 5148–5152.

[27] T. Mokari, C. G. Sztrum, A. Salant, E. Rabani, U. Banin, *Nat. Mater.* **2005**, *4*, 855–863.

[28] S. M. Sze, *Physics of Semiconductor Device*, 2nd ed., Wiley, New York, **1981**, pp. 431–496.

[29] a) R. V. Seidel, A. P. Graham, J. Kretz, B. Rajasekharan, G. S. Duesberg, M. Liebau, E. Unger, F. Kreupl, W. Hoenlein, *Nano Lett.* **2005**, *5*, 147–150; b) A. L. Briseno, J. Aizenberg, Y.-J. Han, R. A. Penkala, H. Moon, A. J. Lovinger, C. Kloc, Z. Bao, *J. Am. Chem. Soc.* **2005**, *127*, 12164–12165; c) S. J. Kang, C. Kocabas, T. Ozel, M.

Shim, N. Pimparkar, M. A. Alam, S. V. Rotkin, J. A. Rogers, *Nat. Nanotechnol.* **2007**, *2*, 230–236; d) A. K. Wanekaya, M. A. Bangar, M. Yun, W. Chen, N. V. Myung, A. Mulchandani, *J. Phys. Chem. A J. Phys. Chem. C.* **2007**, *111*, 5218–5221.

[30] M. D. Curtis, J. Cao, J. W. Kampf, *J. Am. Chem. Soc.* **2004**, *126*, 4318–4328.

[31] a) A. D. Adler, F. R. Longo, J. D. Finarelli, J. Goldmacher, J. Assour, L. Korsakoff, *J. Org. Chem.* **1967**, *32*, 476–476; b) G. D. Dorough, J. R. Miller, F. M. Huennekens, *J. Am. Chem. Soc.* **1951**, *73*, 4315–4320.

[32] a) P. R. Edgington, P. McCabe, C. F. Macrae, E. Pidcock, G. P. Shields, R. Taylor, M. Towler, J. van de Streek, *J. Appl. Crystallogr.* **2006**, *39*, 453–457; b) I. J. Bruno, J. C. Cole, P. R. Edgington, M. K. Kessler, C. F. Macrae, P. McCabe, J. Pearson, R. Taylor, *Acta Crystallogr. Sect. B* **2002**, *58*, 389–397; c) R. Taylor, C. F. Macrae, *Acta Crystallogr. Sect. B* **2001**, *57*, 815–827.

[33] G. M. Sheldrick, *SHELX97. Programs for Crystal Structure Analysis (Release 97–2)*. University of Goettingen, Germany, **1997**.